Journal of Organometallic Chemistry 694 (2009) 3742–3748

Contents lists available at ScienceDirect

Journal of Organometallic Chemistry

journal homepage: www.elsevier.com/locate/jorganchem

Synthesis, photophysical properties, and theoretical studies on pyrrole-containing bromo Re(I) complex

Zhenjun Si [a,b], Xiaona Li [a], Xiyan Li [a], Hongjie Zhang [a,*]

[a] State Key Laboratory of Rare Earth Resource Utilization, Changchun Institute of Applied Chemistry, Chinese Academy of Sciences, Changchun 130022, People's Republic of China
[b] School of Materials Science and Engineering, Changchun University of Science and Technology, Changchun 130022, People's Republic of China

ARTICLE INFO

Article history:
Received 4 May 2009
Received in revised form 22 July 2009
Accepted 24 July 2009
Available online 30 July 2009

Keywords:
Synthesis
Characterization
Re(I) complexes
Phosphorescence

ABSTRACT

Two bromo rhenium(I) carbonyl complexes with the formula of $[Re(CO)_3(\mathbf{L})Br]$, where **L** = 1,10-phenanthroline (**Phen–Re**) and 5-(1H-pyrrol-1-yl)-1,10-phenanthroline (**Pyph–Re**), were successfully synthesized with the aim to analyze the effect of the pyrrole (**Py**) moiety on the photophysical properties of **Pyph–Re**. It was found that the triplet metal-to-ligand charge-transfer $d\pi$ (Re) → π^*(*N-N*) emission of **Phen–Re** and **Pyph–Re** centered at ca. 527 nm with the luminescence quantum yield (LQY) of 0.015 and ca. 578 nm with the LQY of 0.011, respectively. At the same time, the geometrical structures of the ground state and the absorption spectral properties of **Phen–Re** and **Pyph–Re** were also calculated with the 6-31G* basis set employed on C, H, N, O, and Br atoms, and LANL2DZ adopted on Re atom. According to the experimental and theoretical analysis, the red-shift of the photoluminescent spectrum and the lower LQY of **Pyph–Re** should be mainly attributed to the narrower energy gap between the highest occupied molecular orbital and the lowest unoccupied molecular orbital and the more LLCT transition ration of **Pyph–Re**, respectively.

1. Introduction

Since the first report on the electroluminescence (EL) of the Re(I) complexes [1], several groups paid attention to explore novel Re(I) complexes [2–6] with the potential application in EL devices because of these materials' potentiality of achieving an internal quantum efficiency of 100% with the application of triplet irradiative emission. However, the commercial basic materials from which the widely studied chloro Re(I) complexes are synthesized are very expensive, which limits the practical application of this kind of Re(I) complexes. Therefore, the relatively economical bromo Re(I) complexes are considered [5]. In order to improve the photoluminescent (PL) properties and suppress the triplet–triplet annihilation [7,8], different functional groups were applied to synthesize novel bromo Re(I) complexes. The carbazole, a kind of electro-donor group, was reported to be used as the functional group to synthesize bromo Re(I) complexes with the excellent PL properties [9,10]. As can be regarded as the center of the carbazole, the pyrrole (**Py**) ring should exert an influence on the PL properties of the corresponding bromo Re(I) complexes. Therefore, in this article, the bromo Re(I) complexes of [1,10-phenanthroline]$Re(CO)_3Br$ (**Phen–Re**) and **Py**-containing [5-(1H-pyrrol-1-yl)-1,10-phenanthroline]$Re(CO)_3Br$ (**Pyph–Re**) are synthesized by the rational molecule design tactics, and the effect of the **Py** group on the photophysical properties of **Pyph–Re** are experimentally and theoretically studied.

2. Experimental

2.1. Materials and methods

All chemicals are commercially available and used without further purification. The synthesis of 5-amino-1,10-phenanthroline (**Phen–NH_2**) was performed by the nitration of 1,10-phenanthroline in a mixture of concentrated sulfuric acid and fuming nitric acid, followed by the reduction of the nitro derivative with hydrazine over a 5% Pd/C catalyst [11].

2.1.1. Synthesis of 5-(1H-pyrrol-1-yl)-1,10-phenanthroline (*Pyph*)

Phen–NH_2 (0.390 g, 2.0 mmol) and 2,5-dimethoxytetrahydrofuran (DMOTHF) (0.264 g 2.0 mmol) were added into a flask containing 15 mL HOAc, the mixture was refluxed under N_2 for 1 h, then cooled to room temperature (RT). The crude product was poured into 100 mL H_2O and stirred 15 min. The resulting powder was collected by filtration and washed successively with dilute aqueous NaOH solution, H_2O, and methanol to get 0.42 g (85%) of pale yellow powder. ^1H NMR ($CDCl_3$, 400 MHz): δ 6.47 (2H, t, J = 2), 7.04 (2H, t, J = 2), 7.63–7.66 (1H, tetr, J = 4), 7.67–7.70 (1H, tetr, J = 4), 7.81 (1H, s) 8.16 (1H, d, J = 8), 8.27 (1H, d, J = 8)

* Corresponding author. Tel.: +86 431 85262127; fax: +86 431 85698041.
E-mail address: hongjie@ciac.jl.cn (H. Zhang).

0022-328X/$ - see front matter © 2009 Elsevier B.V. All rights reserved.
doi:10.1016/j.jorganchem.2009.07.036

9.22–9.24 (2H, m), Anal. Calc. for $C_{16}H_{11}N_3$: C, 78.35; H, 4.52; N, 17.13. Found: C, 78.69; H, 4.33; N, 16.98%. IR (KBr): ν 743, 1481, 1625, 3085 cm^{-1}.

2.1.2. Synthesis of ***Phen–Re***

Phen (0.036 g, 0.200 mmol), $Re(CO)_5Br$ (0.081 g, 0.200 mmol) and 15 mL toluene were refluxed in a flask for 9 h. After the mixture was cooled to RT, the solvent was removed in a water bath under reduced pressure. The resulting yellow solid was washed with CH_2Cl_2. Yield: 0.085 g (80%). ^1H NMR ($CDCl_3$, 400 MHz): δ 7.87–7.91 (2H, m), 8.045 (2H, s), 8.55–8.57 (2H, tetr), 9.43–9.45 (2H, tetr). Anal. Calc. for $C_{15}H_8BrN_2O_3Re$: C, 33.97; H, 1.52; N, 5.28. Found: C, 34.38; H, 1.24; N, 5.44%. IR (KBr): ν 1425, 1895, 1929, 2017, 3083 cm^{-1}.

2.1.3. Synthesis of ***Pyph–Re***

The procedure is similar to that of **Phen–Re**. Yield: 84%. ^1H NMR ($CDCl_3$, 400 MHz): δ 7.86–7.93 (2H, m), 8.01 (2H, s), 8.48–8.56 (2H, m), 9.44–9.48 (2H, m). Anal. Calc. for $C_{19}H_{11}BrN_3O_3Re$: C, 38.33; H, 1.86; N, 7.06. Found: C, 38.52; H, 1.60; N, 7.27%. IR (KBr): ν 1479, 1894, 1920, 2022, 3047 cm^{-1}.

2.2. Measurements

The IR spectra were acquired using a Magna560 FT-IR spectrophotometer. Element analyses were performed using a Vario Element Analyzer. ^1H NMR spectra were obtained using a Bruker AVANVE 400 MHz spectrometer with tetramethylsilane as the internal standard. The absorption and PL spectra of the degassed solution with 10^{-4} mol/L sample were recorded on a Lambda 750 spectrometer and a Hitachi model F–4500 fluorescence spectrophotometer, respectively. The luminescence quantum yields (LQYs) were measured by comparing fluorescence intensities (integrated areas) of a standard sample (quinine sulfate) and the unknown sample according to the following equation:

$$\Phi_{unk} = \Phi_{std}(I_{unk}/A_{unk})(A_{std}/I_{std})(\eta_{unk}/\eta_{std})^2$$

where Φ_{unk} is the LQY of the unknown sample; Φ_{std} is the LQY of quinine sulfate and taken as 0.546 [12]; I_{unk} and I_{std} are the integrated fluorescence intensities of the unknown sample and quinine sulfate with the excitation wavelength of 400 nm for bromo Re(I) complexes and 364 nm for quinine sulfate. A_{unk} and A_{std} are the absorbances of the unknown sample at 400 nm and quinine sulfate at 364 nm, respectively. The η_{unk} and η_{std} are the refractive indices of the corresponding solvents (pure solvents were assumed). The excited-state lifetimes were detected by a system equipped with a TDS 3052 digital phosphor oscilloscope pulsed Nd:YAG laser with a THG 299 nm output and a computer-controlled digitizing oscilloscope according to the reported method [13]. The ORIGIN 7.0 program by OriginLab Corporation was used for the curve-fitting analysis. The absorption and emission spectral data of **Phen–Re** and **Pyph–Re** in CH_2Cl_2 media and solid state are listed in Table 1.

Cyclic voltammetry measurements were conducted on a voltammetric analyzer (CH Instruments, Model 620B) with a polished Pt plate as the working electrode, Pt mesh as the counter electrode, and a commercially available saturated calomel electrode (SCE) as the reference electrode, at a scan rate of 0.1 V/s. The voltammograms were recorded in CH_3CN solutions with $\sim10^{-3}$ M sample and 0.1 M tetrabutylammonium hexafluorophosphate ($TBAPF_6$) as the supporting electrolyte. In order to precisely calculate the energy levels of the HOMO and the LUMO, the offset potentials are determined by the point of intersection of the tangential lines near the beginning part of the redox peaks. Prior to each electrochemical measurement, the solution was purged with nitrogen for ~10–15 min to remove the dissolved O_2 gas.

2.3. Computational details

The geometrical structures of the ground states were optimized by the density functional theory (DFT) [14] with Becke's LYP (B3LYP) exchange-correlation functional [15]. On the basis of the optimized ground state geometry structures, the absorption spectral properties in CH_2Cl_2 media were calculated by time-dependent DFT (TDDFT) [16] approach associated with the polarized continuum model (PCM) [17]. To investigate solvent effect, the singlet absorption spectra of **Phen–Re** and **PyPh–Re** in the gas phase were also theoretically studied at the same level. The 6-31G* [18–20] basis set was employed on C, H, N, O, and Br atoms, and LANL2DZ basis set was adopted on Re atom. To intuitively understand the transition process, the calculated isosurface plots for the frontier molecular orbitals of **Phen–Re** and **Pyph–Re** involved in the transitions were prepared by using the GAUSSVIEW 3.07 software and shown in Figs. 4 and 5, respectively. All the calculations were performed with the GAUSSIAN 03 software package [21].

3. Results and discussion

3.1. Synthesis and characterization

As depicted in Scheme 1, **Pyph** was synthesized from the reaction between **Phen–NH_2** and DMOTHF in HOAc [22]. **Phen–Re** and **Pyph–Re** were obtained in a previously reported approach [23]. The structures of **Pyph**, **Pyph–Re**, and **Phen–Re** were fully verified with elemental analysis, IR, UV–Vis, and ^1H NMR spectroscopy.

3.2. Photophysical properties

Fig. 1 presents the powder-sample based excitation and PL spectra and the CH_2Cl_2 solution based UV–Vis absorption spectra of **Phen–Re** and **Pyph–Re**. The higher-energy absorption bands of **Phen–Re** and **Pyph–Re** in ca. 230–330 nm region should be assigned to the admixture of ligand-based charge-transfer $\pi \rightarrow \pi^*$ (ILCT/LLCT) transitions, and the lower-energy features in ca. 330–500 nm are tentatively assigned to the metal-to-ligand charge-transfer $d\pi$ (Re) $\rightarrow \pi^*(N\text{-}N)$ (MLCT) transitions. These assignments are confirmed by the UV–Vis absorption spectra of the free ligands and the theoretical calculations (vide infra).

Similar to the previous reports, the broad and lower-energy bands in the absorption spectra partially resolve into two bands in scanning the excitation spectra, namely, ^{1}MLCT transition states with peaks at 390, 410 nm and ^{3}MLCT transition states with peaks

Table 1
Absorption, excitation, and emission spectral parameters of **Phen–Re** and **Pyph–Re** in CH_2Cl_2 and solid state at RT.

Complex	Medium	Absorption	Excitation	Emission	
		λ/nm	λ/nm	λ_{max} ($W_{1/2}$)/nm	φ (degass)
Phen–Re	CH_2Cl_2	267, 292, 377, 411	310, 420	554 (90)	0.015
	Solid		354, 453	527 (76)	
Pyph–Re	CH_2Cl_2	254, 290, 323, 402	372, 464	588 (88)	0.011
	Solid		269, 329, 365, 488	578 (73)	

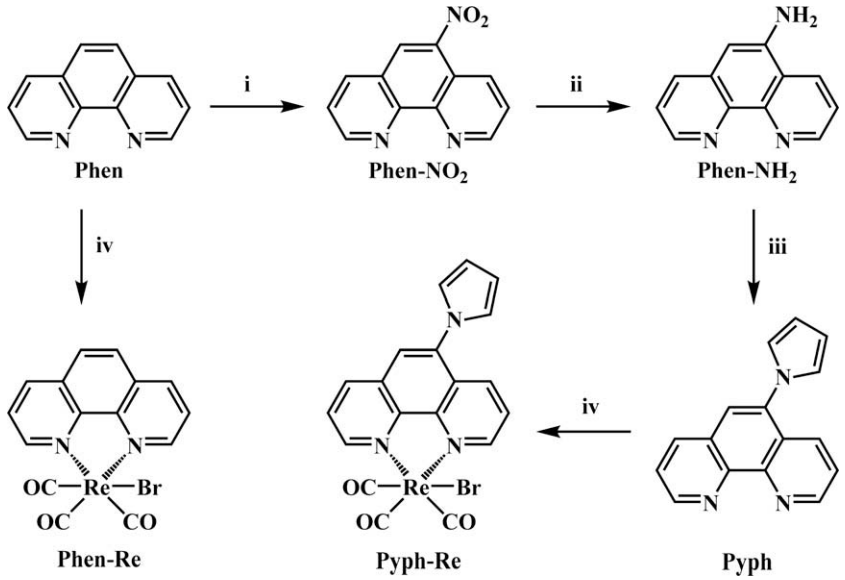

Scheme 1. Synthesis routes of **Phen–Re** and **Pyph–Re**. Reagents and experimental conditions: (i) HNO_3/H_2SO_4, 160–170 °C, 2 h; (ii) hydrazine monohydrate, Pd/C 5%, ethanol, 10 h, N_2; (iii) HOAc, DMOTHF, reflux, 1 h, N_2; (iv) toluene, $Re(CO)_5Br$, 90 °C, 9 h, N_2.

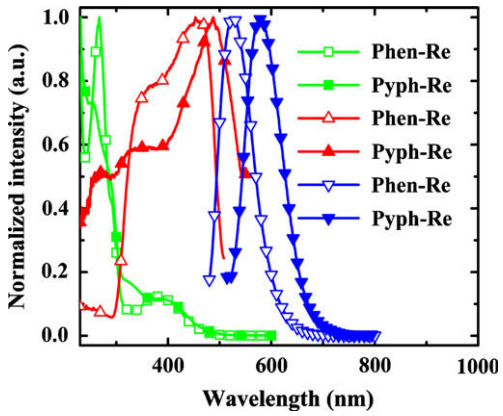

Fig. 1. Absorption (CH_2Cl_2 solution, green), excitation (powder, red), and PL spectra (powder, blue) of **Phen–Re** and **Pyph–Re**. (For interpretation of the references to colour in this figure legend, the reader is referred to the web version of this article.)

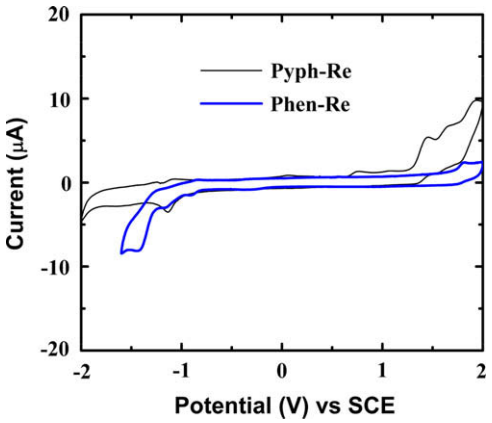

Fig. 2. Cyclic voltammograms of **Phen–Re** and **Pyph–Re** measured in CH_3CN (vs. SCE) at a scan rate of 0.1 V/s. A polished Pt plate and a Pt mesh were used as the working electrode and the counter electrode, respectively. $TBAPF_6$ was taken as the supporting electrolyte.

at 444, 453 nm for **Phen–Re** and **Pyph–Re**, respectively [9,24], and the excitation at either the $\pi \rightarrow \pi^*$ absorption region (~256 nm) or the MLCT absorption region (ca. 453 nm for **Phen–Re** and ca. 488 nm for **Pyph–Re**) at RT leads to the same ^{3}MLCT emission band centered at 525 and 577 nm for **Phen–Re** and **Pyph–Re**, respectively.

The PL spectra of **Phen–Re** and **Pyph–Re** present the emission bands centered at ca. 525 nm with the width of half maximum ($W_{1/2}$) of 76 nm and 577 nm with the $W_{1/2}$ of ca. 73 nm, respectively. At the same time, the LQYs of **Phen–Re** and **Pyph–Re** are measured to be 0.015 and 0.011, respectively. According to the **Phen–Re**, the LLCT transitions should make more contribution to the CT transitions of **Pyph–Re**, which lowers the ratio of MLCT: LLCT during the PL process. Therefore, the lower LQY of **Pyph–Re** should be reasonable. Additionally, the slit rotation of the **Py** group in **Pyph–Re** should also lower its LQY. The red-shift of the PL spectrum of **Pyph–Re** implies that the energy gap between the highest occupied molecular orbital (HOMO) and the lowest unoccupied molecular orbital (LUMO) of **Pyph–Re** should be narrower than that of **Phen–Re**, which is in accordance with the electrochemical analysis.

The cyclic voltammograms of **Phen–Re** and **Pyph–Re** in Fig. 2 exhibit irreversible metal centered oxidation and ligand-based reduction in CH_3CN solution. The peaks of the oxidation process (Re^I/Re^{II}) [25] associated anodic waves of **Phen–Re** and **Pyph–Re** locate at +1.81 V with the onset oxidation potential (V_{onset}) of +1.70 V and +1.45 V with the V_{onset} of +1.31 V, respectively. At the same time, the reduction process ($[Re^IBr(CO)_3(L)]/[Re^IBr(CO)_3(L^{\cdot})]^-$) associated cathodic waves of **Phen–Re** and **Pyph–Re** peak at −0.91 V with V_{onset} of −0.81 V and −1.14 V with V_{onset} of −0.95 V, respectively. The energy levels of the HOMO (E_{HOMO}) and the LUMO (E_{LUMO}) are calculated from the onset oxidation (E_{onset}(Ox)) and reduction (E_{onset}(Red)) potentials with the formula of $E_{HOMO} = -4.74 - E_{onset}(Ox)$ and $E_{LUMO} = -4.74 - E_{onset}(Red)$ (−4.74 V for SCE with respect to the zero vacuum level [26]). These calculations give the E_{HOMO} of −6.44 and −6.05 eV, and the E_{LUMO} of −3.94 and −3.79 eV for **Phen–Re** and **Pyph–Re**, respectively. The energy gaps of **Phen–Re** and **Pyph–Re** are measured to be 2.50 and 2.26 eV, respectively, indicating that the red-shift of the PL spectrum of **Pyph–Re** should be reasonable.

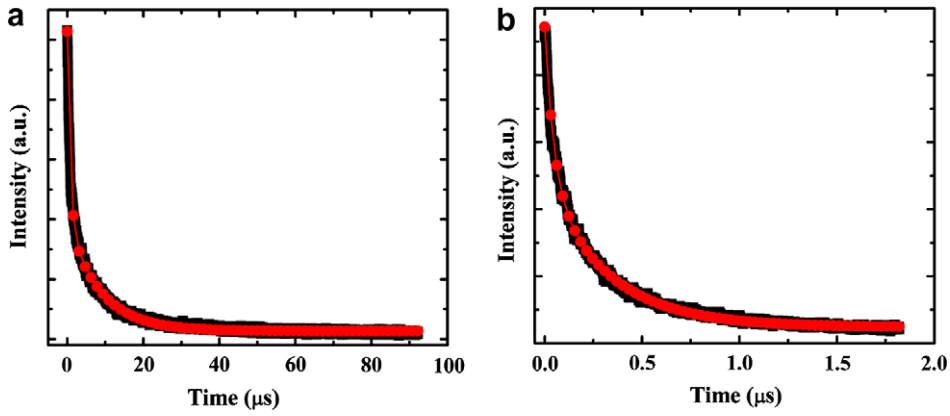

Fig. 3. PL lifetime decay measurements of the powder samples of **Phen–Re** (a) and **Pyph–Re** (b).

The potential surface crossing (PSC) from the higher $\pi \rightarrow \pi^*$ state to the lower MLCT state of **Phen–Re** and **Pyph–Re** is also analyzed by the measurements of their excited-state lifetimes [27]. As indicated in Fig. 3, the biexponential decay lifetimes (τ) of **Phen–Re** and **Pyph–Re** are composed of $\tau_1 = 0.749$ ($A_1 = 3.16$), 0.0046 μs ($A_1 = 0.56$) and $\tau_2 = 8.59$ ($A_2 = 1.85$), 0.32 μs ($A_2 = 3.26$), respectively. In general, the observation of the strong excitation bands in the $\pi \rightarrow \pi^*$ absorption region and the shorter decay lifetime from the $\pi \rightarrow \pi^*$ state than those from the lower MLCT state [28] can suggest the efficient PSC from the higher $\pi \rightarrow \pi^*$ state to the lower MLCT state. As can be seen from Fig. 2, the strength of the excitation peaks of **Pyph–Re** are much stronger than those of **Phen–Re** in the $\pi \rightarrow \pi^*$ absorption region with the normalization according to the maximum absorption, suggesting that the efficiency of PSC from the higher $\pi \rightarrow \pi^*$ state to the MLCT state of **Pyph–Re** should be much higher than that of **Phen–Re**. Therefore, the assignment of τ_1 (the major short-lived component of **Phen–Re** and the minor long-lived component of **Pyph–Re**) to the emission from the $\pi \rightarrow \pi^*$ state should be believable. These results suggest that the **Py** moiety in **Pyph–Re** should be beneficial to the PSC from the higher $\pi \rightarrow \pi^*$ state to the lower MLCT state.

3.3. Theoretical calculations

As can be seen from the selective simulated absorption parameters listed in Table 2 and the optimized ground state geometry structures presented in Figs. 4 and 5, the LUMO–LUMO + 2 for both species are mainly composed of the π^* orbital localized on the **Phen** moiety with $\geqslant$89.8% composition and are a little affected by the **Py** moiety. The HOMO and HOMO–1 of **Phen–Re** and **Pyph–Re** are mainly composed of the Re d orbital and the π-orbital localized on CO and Br moieties. The composition of the HOMO–2 of **Phen–Re** locates at the orbitals of π (CO) and d (Re), while that of **Pyph–Re** mainly locates at the π-orbital of the **Py** moiety. The HOMO–3 of **Phen–Re** is mainly comprised of the π-orbital localized on the whole molecule and that of **Pyph–Re** has the similar distribution to the HOMO–2 of **Phen–Re**. These results present that the **Py** moiety in **Pyph–Re** leads to the different distribution of the HOMO–2 and HOMO–3 between **Phen–Re** and **Pyph–Re**, which should partly contributes to the different photophysical properties between **Phen–Re** and **Pyph–Re**. At the same time, the **Py** moiety in **Pyph–Re** exerts a little effect on the composition of other frontier molecular orbitals presented in Table 3. The E_{HOMO} and E_{LUMO} of **Phen–Re** (**Pyph–Re**) are calculated to be −5.51 (−5.46) and −2.76 (−2.68) eV (Table 3), respectively, and the energy gaps are calculated to be 2.78 and 2.75 eV for **Phen–Re** and **Pyph–Re**, respectively, which is theoretically verified that the PL spectrum of **Pyph–Re** should exhibits a lower-energy properties.

The curves of the theoretically simulated absorption spectra of **Phen–Re** and **Pyph–Re** in CH_2Cl_2 media and the gas phase are presented in Fig. 6, and their selective parameters are listed in Table 2. In general, the two complexes show a blue-shift in CH_2Cl_2 solution compared with those in the gas phase. This is in agreement with the reports from Lu et al. [29], who pointed out that when the polarity of the solvent increases from benzene to CH_2Cl_2, acetonitrile, and ethanol, the broad low-energy absorption band blue-shifts. Taking **Pyph–Re** as an example, the S_1 absorption band shows a comparatively strong solvent-dependent effect: the absorption at 614 nm in the gas phase corresponds to that at 485 nm in CH_2Cl_2 solution. To the transitions mainly assigned to $\pi \rightarrow \pi^*$ characters, the solvent effect is minor [30]. The calculated results in solution are more in agreement with the experimental values, therefore, the later discussions will focus on the results in the CH_2Cl_2 solution.

Table 2
Selected absorptions parameters of **Phen–Re** and **Pyph–Re** in CH_2Cl_2 according to TDDFT (LANL2DZ) calculations.

Complex	State	Transition	λ (nm)/E (eV)	Oscillator	Assign	λ_{exp} (nm)
Phen–Re	S_1	H → L (100%)	474/2.61	0.0010	MLCT/LLCT	434
	S_3	H → L+1 (100%)	427/2.90	0.0092	MLCT/LLCT	
	S_7	H−3 → L (90%)	335/3.70	0.0663	MLCT/LLCT/ILCT	375
	S_{23}	H−6 → L (44%)	262/4.73	0.3500	ILCT	267
	S_{37}	H−4 → L+2 (53%)	236/5.26	0.1545	MLCT/LLCT	
	S_{41}	H−5 → L+2 (59%)	219/5.65	0.1352	MLCT/LLCT	
Pyph–Re	S_1	H → L (100%)	485/2.55	0.0009	MLCT/LLCT	452
	S_{10}	H−3 → L+1 (56%)	346/3.59	0.1037	MLCT	
	S_{12}	H−6 → L (79%)	331/3.75	0.0868	MLCT/LLCT/ILCT	329
	S_{30}	H−9 → L+1 (35%)	259/4.78	0.2308	LLCT/ILCT	257
	S_{34}	H−3 → L+3 (37%)	251/4.94	0.3064	MLCT/LLCT	
	S_{62}	H−6 → L+5 (24%)	211/5.87	0.0959	LLCT/ILCT	

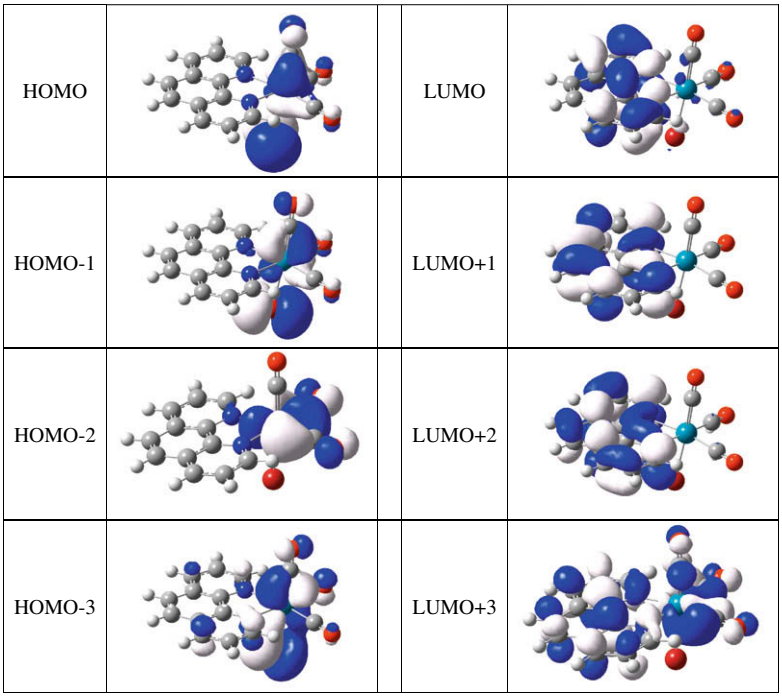

Fig. 4. Calculated isosurface plots for the frontier orbitals of **Phen–Re** in gas phase at the B3LYP/LANL2DZ level.

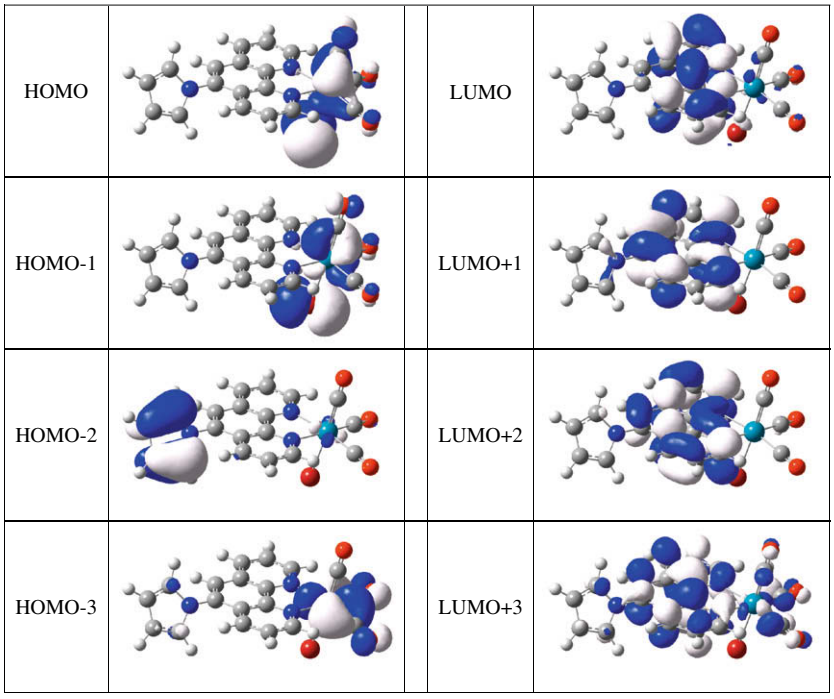

Fig. 5. Calculated isosurface plots for the frontier orbitals of **Pyph–Re** in gas phase at the B3LYP/LANL2DZ level.

As can be seen from Fig. 6, the simulated curves of the absorption spectra of **Phen–Re** and **Pyph–Re** are nicely fitted to those from the experimental measurements. The lowest lying singlet → singlet absorptions of **Phen–Re** and **Pyph–Re** are calculated at 474 and 485 nm, respectively. As presented in Table 2, the configuration of HOMO → LUMO is responsible for both of the lowest lying transitions. Table 3 shows that the HOMO of **Phen–Re** is mainly composed of ca. 20.9% Re(I) d_{yz} orbital, 14.4% carbonyl group, and 55.2% bromine, and the LUMO of **Phen–Re** is a π^* (**Phen**, 89.8%) type orbital. Thus, the lowest lying transitions of **Phen–Re** and **Pyph–Re** should be described as [d(Re) + π(CO + Br)] → [π^*(L)] in nature with MLCT/LLCT characters.

The transitions at the largest oscillator strength with the configurations of HOMO−6 → LUMO (44%) and HOMO−3 → LUMO (37%) contribute to the higher-energy absorption of **Phen–Re** (262 nm) and **Pyph–Re** (251 nm), which are in good agreement with the experimental values of 267 and 257 nm, respectively. The HOMO−6 of **Phen–Re** and the HOMO−3 of **Pyph–Re** are π (**Phen**,

Table 3
Frontier molecular orbital compositions (%) in the ground states for **Phen–Re** and **Pyph–Re** at B3LYP/LANL2DZ level.

Orbital	**Phen–Re**						**Pyph–Re**					
	E (eV)	Bond type	Contribution (%)				*E* (eV)	Bond type	Contribution (%)			
			Re	CO	Br	**Phen**			Re	CO	Br	**Pyph**
LUMO+2	−1.29	π*(L)				95.0	−1.41	π*(L)				92.2**Phen**
LUMO+1	−2.57	π*(L)				99.3	−2.68	π*(L)				96.1**Phen**
LUMO	−2.68	π*(L)				89.8	−2.76	π*(L)				88.9**Phen**
HOMO	−5.46	d(Re) π(CO + Br)	20.9 d_{yz}	14.4	55.2		−5.51	d(Re) π(CO + Br)	18.7 d_{yz}	13.9	56.9	
HOMO−1	−5.50	d(Re) π(CO + Br)	17.8 d_{xz}	11.3	58.4		−5.56	d(Re) π(CO + Br)	16.0 d_{xz}	10.8	59.9	
HOMO−2	−6.36	d(Re) π(CO)	65.7 $d_{x^2-y^2}$	28.4			−6.38	π(L)				87.9**Py**
HOMO−3	−6.63	d(Re) π(CO + Br + L)	24.9 d_{xz}	14.7	36.8	15.1	−6.41	d(Re) π(CO)	41.2 $d_{x^2-y^2}$	27.4		

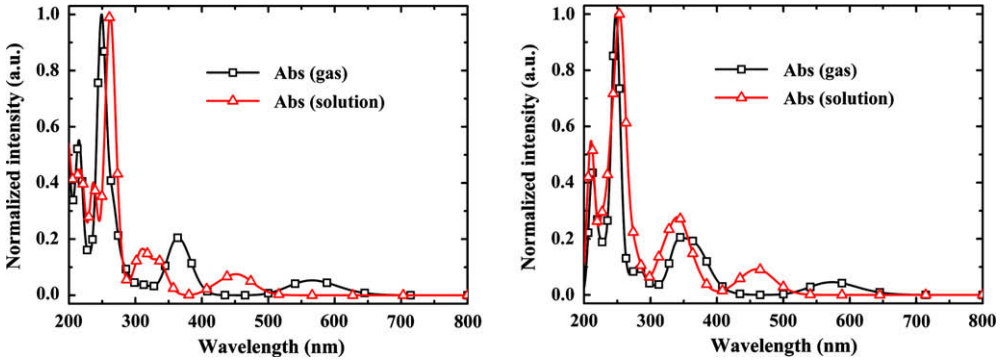

Fig. 6. Simulated absorption spectra in CH_2Cl_2 media and gas phase for **Phen–Re** (left) and **Pyph–Re** (right) calculated at the TDDFT (B3LYP)/LANL2DZ level.

82.9%) and [d (Re, 68.8%) + π (CO, 27.4%)] orbitals in nature, respectively, thus these higher-energy absorptions are attributed to the ILCT and MLCT/LLCT characters, respectively. At the same time, the absorptions with moderate oscillator of **Phen–Re** and **Pyph–Re** are calculated to be the MLCT/LLCT or MLCT/LLCT/ILCT characters.

De Angelis et al. [31] and Chou, Chi et al. [32–34] found that the efficient energy intersystem crossing from the LLCT states to the MLCT states could notably enhances the MLCT participation, namely, the phosphorescence ($T_1 \rightarrow S_0$ radiative transition) should be greatly enhanced by increasing the ratio of MLCT: LLCT. Additionally, Abrahamsson et al. concluded that the LQY could be increased by larger MLCT excited-state compositions [35]. These conclusions are consistent with our calculated results. **Phen–Re** possesses more MLCT composition than **Pyph–Re**, which leads to the fact that the LQY of **Phen–Re** (0.015) are higher than that of **Pyph–Re** (0.011). This result is also proved by the calculated transition moments of **Phen–Re** (1.825) and **Pyph–Re** (1.479) based on the fact that the larger transition moments present the higher transition probability from the ground state to the excited-state and results in the greater emission probability [36].

In conclusion, the photophysical behaviors of two bromo Re(I) complexes of **Phen–Re** and **Pyph–Re** are experimentally and theoretically studied to analyze the effect of the **Py** moiety on the photophysical properties of **Pyph–Re**. It is experimentally found that **Phen–Re** and **Pyph–Re** present the ^{3}MLCT emission centered at ca. 527 nm with LQY of 0.015 and ca. 578 nm with LQY of 0.011, respectively. These results verify that the **Py** group in **Pyph–Re** leads to the more LLCT transitions during the PL process which lowers the LQY of **Pyph–Re**. The ground state molecular structures and the UV–Vis absorption behaviors of **Phen–Re** and **Pyph–Re** are theoretically studied, which are in good agreement with the experimental measurements. Together with the previous studies on the light-emitting bromo Re(I) complexes containing carbazole groups, this study further suggests that the functional groups with bigger steric and conjugated effect should be helpful to improve the photophysical properties of bromo Re(I) complexes.

Acknowledgments

The authors are grateful to the financial aid from the National Natural Science Foundation of China (Grant Nos. 20631040 and 20771099) and the MOST of China (Grant Nos. 2006CB601103 and 2006DFA42610).

References

[1] X. Gong, P.K. Ng, W.K. Chan, Adv. Mater. 10 (1998) 1337.
[2] Y. Li, Y. Liu, J. Guo, F. Wu, W. Tian, B. Li, Y. Wang, Synth. Met. 118 (2001) 175.
[3] C. Fu, M. Li, Z. Su, Z. Hong, W. Li, B. Li, Appl. Phys. Lett. 88 (2006) 093507.
[4] Y. Ma, H. Zhang, J. Shen, C.-M. Che, Synth. Met. 94 (1998) 245.
[5] K. Wang, L. Huang, L. Gao, L. Jin, C. Huang, Inorg. Chem. 41 (2002) 3353.
[6] G. David, P.J. Walsh, K.C. Gordon, Chem. Phys. Lett. 383 (2004) 292.
[7] M.E. Thompson, S.R. Forrest, Nature 395 (1998) 151.
[8] H. Xia, M. Li, D. Lu, C. Zhang, W. Xie, X. Liu, B. Yang, Y. Ma, Adv. Funct. Mater. 17 (2007) 1757.
[9] Z. Si, J. Li, B. Li, F. Zhao, S. Liu, W. Li, Inorg. Chem. 46 (2007) 6155.
[10] X. Li, X. Liu, Z. Wu, H.-J. Zhang, J. Phys. Chem. A 112 (2008) 11190.
[11] K. Binnemans, P. Lenaerts, K. Driesen, C.G. Walrand, J. Mater. Chem. 14 (2004) 191.
[12] K. Ye, J. Wang, H. Sun, Y. Liu, Z. Mu, F. Li, S. Jiang, J. Zhang, H. Zhang, Y. Wang, C.-M. Che, J. Phys. Chem. B 109 (2005) 8008.
[13] J.M. Villegas, S.R. Stoyanov, D.P. Rillema, Inorg. Chem. 41 (2002) 6688.
[14] E. Runge, E.K.U. Gross, Phys. Rev. Lett. 52 (1984) 997.
[15] S.L. Mayo, B.D. Olafso, W.A. Goddard, J. Phys. Chem. 94 (1990) 8897.
[16] J. Autschbach, T. Ziegler, S.J.A. Gisbergen, E.J. Baerends, J. Chem. Phys. 116 (2002) 6930.
[17] M. Cossi, V. Barone, B. Mennucci, Tomasi, J. Chem. Phys. Lett. 286 (1998) 253.
[18] J. Tortajada, A. Total, J.P. Morizur, M. Alcamí, O. Mö, M. Yãez, J. Phys. Chem. 96 (1992) 8309.
[19] A.E. Ketvirtis, V.I. Baranov, A.C. Hopkinson, D.K. Bohme, J. Phys. Chem. A 101 (1997) 7258.
[20] P.N. Simões, L.M. Pedroso, A.M.M. Beja, M.R. Silva, E. MacLean, A.A. Portugal, J. Phys. Chem. A 111 (2007) 150.
[21] M.J. Frisch, G.W. Trucks, H.B. Schlegel, G.E. Scuseria, M.A. Robb, J.R. Cheeseman, J.A. Jr. Montgomery, T. Vreven, K.N. Kudin, J.C. Burant, J.M. Millam, S.S. Iyengar,

J. Tomasi, V. Barone, B. Mennucci, M. Cossi, G. Scalmani, N. Rega, G.A. Petersson, H. Nakatsuji, M. Hada, M. Ehara, K. Toyota, R. Fukuda, J. Hasegawa, M. Ishida, T. Nakajima, Y. Honda, O. Kitao, H. Nakai, M. Klene, X. Li, J.E. Knox, H.P. Hratchian, J.B. Cross, C. Adamo, J. Jaramillo, R. Gomperts, R.E. Stratmann, O. Yazyev, A.J. Austin, R. Cammi, C.J. Pomelli, W. Ochterski, P.Y. Ayala, K. Morokuma, G.A. Voth, P. Salvador, J.J. Dannenberg, V.G. Zakrzewski, S. Dapprich, A.D. Daniels, M.C. Strain, O.D. Farkas, K.A. Malick, D. Rabuck, K. Raghavachari, J.B. Foresman, J.V. Ortiz, Q. Cui, A.G. Baboul, S. Clifford, J. Cioslowski, B.B. Stefanov, G. Liu, A. Liashenko, P. Piskorz, I. Komaromi, R.L. Martin, D.J. Fox, T. Keith, M.A. Al-Laham, C.Y. Peng, A. Nanayakkara, M. Hallacombe, P.M.W. Gill, B. Johnson, W. Chen, M.W. Wong, C. Gonzalez, J.A. Pople, GAUSSIAN 03, Revision C. 02, Gaussian, Inc., Wallingford, CT, 2004.

[22] A.D. Josey, W.G. Dauben, J. Hostynek, Org. Synth. 5 (1973) 716.

[23] C.B. Liu, J. Li, B. Li, Z.R. Hong, F.F. Zhao, S.Y. Liu, W.L. Li, Chem. Phys. Lett. 435 (2007) 54.

[24] S. Ranjan, S.-Y. Lin, K.C. Hwang, Y. Chi, W.-L. Ching, C.-S. Liu, Y.-T. Tao, C.-H. Chien, S.-M. Peng, G.-H. Lee, Inorg. Chem. 42 (2003) 1248.

[25] S. Berger, A. Klein, W. Kaim, J. Fiedler, Inorg. Chem. 37 (1998) 5664.

[26] D.G. Wu, C.H. Huang, L.B. Gan, J. Zheng, Y.Y. Huang, W. Zhang, Langmuir 15 (1999) 7276.

[27] L. Sacksteder, A.P. Zipp, E.A. Brown, J. Streich, J.N. Demas, B.A. DeGraff, Inorg. Chem. 29 (1990) 4335.

[28] D.R. Striplin, G.A. Crossby, Coord. Chem. Rev. 211 (2001) 163.

[29] W. Lu, B.-X. Mi, M.C.W. Chan, Z. Hui, C.-M. Che, N. Zhu, S.-T. Lee, J. Am. Chem. Soc. 126 (2004) 4958.

[30] F. De Angelis, S. Fantacci, A. Selloni, Chem. Phys. Lett. 389 (2004) 204.

[31] F. De Angelis, S. Fantacci, N. Evans, C. Klein, S.M. Zakeeruddin, J.-E. Moser, K. Kalyanasundaram, H.J. Bolink, M. Grätzel, M.K. Nazeeruddin, Inorg. Chem. 46 (2007) 5989.

[32] P.T. Chou, Y. Chi, Chem. Eur. J. 13 (2007) 380.

[33] Y. Chi, P.T. Chou, Chem. Soc. Rev. 36 (2007) 1421.

[34] E.Y. Li, Y.M. Cheng, C.C. Hsu, P.T. Chou, G.H. Lee, I.H. Lin, Y. Chi, C.S. Liu, Inorg. Chem. 45 (2006) 8041.

[35] M. Abrahamsson, L. Hammarström, D.A. Tochere, S. Nag, D. Datta, Inorg. Chem. 45 (2006) 9580.

[36] T.Y. Chu, M.H. Ho, J.F. Chen, C.H. Chen, Chem. Phys. Lett. 415 (2005) 137.